

One-dimensional modeling of bulk cationic interdiffusion in mixed oxides (U,Pu)O_2 and analysis of homogenization within a microstructure using a finite difference method

Nadia Dempowo, François Valdivieso, Julien Bruchon, Jacques Lechelle

▶ **To cite this version:**

Nadia Dempowo, François Valdivieso, Julien Bruchon, Jacques Lechelle. One-dimensional modeling of bulk cationic interdiffusion in mixed oxides (U,Pu)O_2 and analysis of homogenization within a microstructure using a finite difference method. Journal of Nuclear Materials, 2022, 568, pp.153850. 10.1016/j.jnucmat.2022.153850 . cea-03713932

HAL Id: cea-03713932
https://cea.hal.science/cea-03713932

Submitted on 5 Jul 2022

HAL is a multi-disciplinary open access archive for the deposit and dissemination of scientific research documents, whether they are published or not. The documents may come from teaching and research institutions in France or abroad, or from public or private research centers.

L'archive ouverte pluridisciplinaire **HAL**, est destinée au dépôt et à la diffusion de documents scientifiques de niveau recherche, publiés ou non, émanant des établissements d'enseignement et de recherche français ou étrangers, des laboratoires publics ou privés.

A ONE-DIMENSIONAL MODELING OF U/Pu INTERDIFFUSION IN MIXED OXIDES $(U,Pu)O_2$ AND ANALYZIS OF HOMOGENIZATION WITHIN A MICROSTRUCTURE USING A FINITE DIFFERENCE METHOD

Nadia Curie DEMPOWO [1,2], François VALDIVIESO[2], Julien BRUCHON[2], Jacques LECHELLE[1]

[1] CEA/DES/IRESNE/DEC/SESC/LM2C, Site de Cadarache- Bât 151, 13108 Saint-Paul Lez Durance, France

[2]Mines Saint-Etienne, Univ Lyon, CNRS, UMR 5307 LGF, Centre SMS, F - 42023 Saint-Etienne, France

Abstract

This paper deals with the interdiffusion phenomena, which take place during the solid state sintering of nuclear fuel mixed oxides. Interdiffusion occurs on both sides of neighboring grains (or crystallites of the starting powders) with different initial chemical composition (either UO_2 or PuO_2): it occurs because one or more grain boundaries separate grains with different initial chemical compositions. The objective of this work is to study numerically the interdiffusion in two grains in one dimension. The numerical method used is the finite difference method applied to the Fick's laws for multicomponent systems. The concentration profiles of uranium and plutonium are plotted versus time to analyze and understand the evolution of each element in the single-crystals. Neumann boundary conditions better represent the physical reality of interdiffusion of mixed oxides due to the limited spatial extent of the initial crystallites. In the simulations, pure UO_2 and PuO_2 crystallites are brought into contact at the initial time. After four hours (typical duration of sintering), each diffusing element is distributed over the full length formed by the two interdiffusion half-couples. Moreover, the phenomenon of homogenization has been also analyzed within two kinds of microstructures: first, a unimodal size distribution of single-crystals, second, a non-unimodal size distribution of single-crystals. In order to carry out the numerical study of the homogenization phenomenon within these two microstructures, the standard deviation of the concentration of U or Pu criterion is used, which makes it possible to analyze the homogeneity degree of the system after a certain period of time, as well as the time necessary to reach a given homogeneity. This time is longer when the crystals are the largest.

Keywords: Modeling, Interdiffusion, MOX, homogenization, microstructure, finite difference

1. Introduction

Sintering is a process frequently encountered in the manufacturing process of ceramics materials. The sintering of ceramics constituted by only one chemical element is a non-reactive sintering. However, very often, ceramics are constituted by more than one chemical element and are therefore heterogeneous from a chemical point of view. Reactive sintering has long been successfully experimentally used in the field of traditional ceramics and has been developed for technical ceramics since the last quarter of the last century. Mullite-zirconia is often used as a model system [1-5]. Sintering is a key step in the manufacturing process of mixed oxides used as fuels in nuclear reactors. Since Pu has been reprocessed as MOX fuel, the sintering stage has become a reactive sintering in which a chemical reaction between the initial constituents of the green compact (made of UO_2 and PuO_2 powders) and its densification occurs during the same thermal treatment. So far, in order to construct a sintering model, all numerical studies have supposed that the ceramics are homogeneous [6–10]. Unlike these latter, the sintering of mixed oxides is reactive, due to the number of chemical elements in presence, precisely uranium, plutonium and oxygen. A sub-granular model for solid state free sintering of mixed oxides has been developed in order to follow the evolution of two grains in references [11–13]. This model, named SALAMMBO, describes the behavior of two grains by solving Fick's laws with fluxes arising from different diffusion mechanisms (grain boundary, surface and volume). In addition to the chemical origin of diffusion, a mechanical part leading to shrinkage is considered. In fact, the flux is written $\vec{j} = -L\vec{\nabla}\frac{\mu}{T}$. The chemical potential in this equation consists of a mechanical and a chemical part. This means $\mu = \mu_{mecha} + \mu_{chem}$ with $\mu_{mecha} = -\frac{\Omega}{2}\left(\bar{\bar{\sigma}} : \bar{\bar{\varepsilon}}\right)$ where $\bar{\bar{\sigma}}$ stands for the stress field whereas $\bar{\bar{\varepsilon}}$ stands for the strain field and μ_{chem} is constant (taken as zero) when the material is homogeneous (current SALAMMBO consideration) and varying when the material is heterogeneous (MOX case). The Navier-Lame equations are solved at each time step in the bulk of each grain, providing the 3D-displacement field and hence the density of the elastic mechanical energy. The gradient of energy is the driving force of diffusion phenomena occurring during densification. As any other sintering model, this model was first developed for the simplified case of a chemically homogeneous material. As $(U,Pu)O_2$ ceramics are initially heterogeneous and homogeneity of nuclear is required to avoid localized high burnup areas during irradiation, it is necessary to take into account the bulk diffusion of each of the three chemical elements in order to construct a reactive sintering model of $(U,Pu)O_2$. The understanding of this reactive sintering can help to improve cationic homogenization experimental conditions. To do so, the interdiffusion mechanism which is one of the physical phenomena involved and which conditions the formation of the $(U,Pu)O_2$ solid solution requires attention.

This reactive sintering supposes to solve Fick's laws not only for each diffusion mechanism, but also for each chemical element. Some studies in the literature deal with the resolution of Fick's laws in the binary or ternary systems depending on their aims. In a binary system, only one diffusion coefficient comes into play. In contrast, in a ternary system in which two or more cations are being transported, new complications arise : a single interdiffusion coefficient is no longer appropriate to describe the diffusion process [14,15]. This makes the use of a diffusion matrix necessary [16]. The diffusion matrix contains four diffusion coefficients namely the "main-term" diffusion coefficients (for diagonal ones) and "cross-term" diffusion coefficients (for off-diagonal ones). In general, the cross-terms are not symmetric. Some works reported in the literature neglect the cross-terms [17,18]. Such an approximation cannot be made for U-Pu interdiffusion because these cations diffuse on the same cationic sites of the fluorine structure with a trace amount of cationic vacancies. A non-zero value of a cross-term gives a measure of a flux of one component generated by the concentration gradient of a second component. That means the multicomponent diffusion is a non-linear problem and the interactions between components are significant.

The

The

2. Methodology

2.1. Multicomponent flux equations: the ternary system (U,Pu,O)

Fick's laws expressing the fluxes of species account for diffusion phenomena. In the context of interdiffusion, the process consists in bringing two single-crystals into contact. Each single-crystal has its own initial chemical composition. In the context of MOX sintering, UO_2 and PuO_2 are brought into contact, so that there are three chemical elements U, Pu and O and m

u

l

t

i

c

o

m

p

o

n

e

n

t

d

i

f

f

u

s

i

o

n

a

n

d

t

h

e

r

m

o

d

y

n

a

m

i

c

d

e

s

c

r

i

p

t

i

o

n

.

R

E

F

$$\boldsymbol{J_k} = -\sum_{\boldsymbol{j=1}}^{\boldsymbol{n-1}} \boldsymbol{D_{kj}^n \nabla c_j} \qquad (1)$$

$$\frac{\partial c_k}{\partial t} = -\nabla . \boldsymbol{J_k} \qquad (2)$$

where J_k represents the diffusional flux of the chemical element k; n stands for the number of chemical element in the system; c_k is the concentration of the chemical element k; and $\boldsymbol{D_{kj}^n}$ is the diffusivity that can be expressed as [30]:

$$D_{kj}^n = D_{kj} - D_{kn}\left(\frac{V_j}{V_n}\right) \qquad (3)$$

where V_j represents the partial volume of chemical element j and V_n is the total volume of the pattern (i.e one mole of $U_{1-x}Pu_xO_2$).

In addition,

$$D_{kj} = \sum_{i=1}^{n} (\delta_{ik} - x_k) x_i M_i \frac{\partial \boldsymbol{\mu_i}}{\partial x_j} \qquad (4)$$

Here x_k is the mole fraction of chemical element k, δ_{ik} represents the Kronecker symbol, equal to 1 if $i=k$, and 0 to otherwise. $\frac{\partial \boldsymbol{\mu_i}}{\partial x_j}$ is the partial derivative of the chemical potential of the species i with respect to the mole fraction x_i and corresponds to the thermodynamic factor of Darken. This quantity can therefore be evaluated from the thermodynamic description of the system. The expressions for the chemical potentials must be given in the form $\mu_k(x_1, x_2, \ldots, x_n)$. M_i represents the mobility of element i. In this framework, there is no question of determining diffusion coefficients from mobilities and the thermodynamic model of the solid solution; these values will be obtained by interpolating experimental data.

$\boldsymbol{Jk} = -\sum_{\boldsymbol{j=1}}^{\boldsymbol{n-1}} \boldsymbol{D_{kj}^n \nabla c_j}$, which gives the expression of flux, has a limit: one of the elements is not taken into account into the summation. The choice of the last element that is excluded in the computation of interdiffusion flux depends on the type and the characteristics of the system. Generally, in the systems build up of solute and solvent, the flux of solvent is neglected. So, we will determine in the n-component system, (n-1) interdiffusion fluxes and (n-1) interdiffusion coefficients. In addition, in the volume center frame, the fluxes are related to each other and we can numerically deduce the flux of the last element (n-component) as $\sum_{\boldsymbol{i=1}}^{\boldsymbol{3}} \boldsymbol{V_i J_i = 0}$ [16]. Therefore, as explained in the introduction, Fick's laws will apply on U and Pu and the flux of O could be deduced if necessary from this relation.

In order to simulate 1D interdiffusion, the two Fick's laws are combined to determine the concentrations, leading to:

$$\frac{\partial c_k}{\partial t} = \sum_{j=1}^{n-1} D_{kj}^n \frac{\partial^2 c_j}{\partial x^2} \qquad (5)$$

R

E

F

R

2.2. Physical model

Depar

$$\frac{\partial c_k}{\partial t} = \sum_{j=1}^{n-1} D_{kj}^{n} \frac{\partial^2 c_j}{\partial x^2} \Rightarrow \begin{cases} \frac{\partial c_U}{\partial t} = D_{UU}^{O} \frac{\partial c_U}{\partial x^2} + D_{UPu}^{O} \frac{\partial c_{Pu}}{\partial x^2} \\ \frac{\partial c_{Pu}}{\partial t} = D_{PuU}^{O} \frac{\partial c_U}{\partial x^2} + D_{PuPu}^{O} \frac{\partial c_{Pu}}{\partial x^2} \end{cases} \Rightarrow \frac{\partial c}{\partial t} = D \frac{\partial^2 c}{\partial x^2} \quad (6)$$

ting for

with $D = \begin{pmatrix} D_{UU}^{O} & D_{UPu}^{O} \\ D_{PuU}^{O} & D_{PuPu}^{O} \end{pmatrix}$ and $c = \begin{pmatrix} c_U \\ c_{Pu} \end{pmatrix}$; thus, the matrix D is diagonalized, using the eigenvector matrix B and the eigenvalue diagonal matrix λ. The relations between the matrices B, D, c, c' and λ are:

mo

$$\begin{matrix} c' = B^{-1}c \\ DB = B\lambda \end{matrix} \Rightarrow \frac{\partial c'}{\partial t} = \lambda \frac{\partial^2 c'}{\partial x^2} \quad (7)$$

the

with $c' = \begin{pmatrix} c'_U \\ c'_{Pu} \end{pmatrix}$. Let us express the components of matrices B and λ:

equ

$B = \begin{pmatrix} b_{UU} & b_{UPu} \\ b_{PuU} & b_{PuPu} \end{pmatrix}$ and $\lambda = \begin{pmatrix} \lambda_U & 0 \\ 0 & \lambda_{Pu} \end{pmatrix}$

ation

with $b_{UU} = 1$, $b_{UPu} = \frac{D_{UU} - \lambda_U}{D_{PuU}}$, $b_{PuU} = \frac{D_{PuU}}{D_{UU} - \lambda_{Pu}}$, $b_{PuPu} = 1$,

$$\lambda_U = \frac{1}{2}(D_{UU} + D_{PuPu} - \sqrt{(D_{UU} - D_{PuPu})^2 + 4D_{PuU} D_{UPu}}$$

$$\lambda_{Pu} = \frac{1}{2}(D_{UU} + D_{PuPu} + \sqrt{(D_{UU} - D_{PuPu})^2 + 4D_{PuU} D_{UPu}}$$

resu

The values of interdiffusion coefficients are obtained by interpolating Matzke graph [31] that gives the representation of interdiffusion coefficient at T=1600°C with an oxygen potential of ~90 kcal/mol (~ -375kJ/mol). The magnitude order is around 10^{-4}cm²/s. Thus, for the modeling of the interdiffusion between the couple UO_2/PuO_2, the following diffusion coefficients will be used: $D_{UU}^{O} = 6*10^{-14}\ cm^2/s$, $D_{PuPu}^{O} = 12*10^{-14}\ cm^2/s$, $D_{UPu}^{O} = 10^{-14}\ cm^2/s$, $D_{PuU}^{O} = 2*10^{-14}\ cm^2/s$.

lt

Furthermore, for the modeling of the interdiffusion between the couple of two pellets $UO_2/U_{0.55}Pu_{0.45}O_2$, the magnitude order provided by the plot of Noyau [28], for a value of oxygen potential of -395 kJ.mol^{-1}, will be used. The values that will be considered to reproduce the concentration profile of UO_2 are: $D_{UU}^{O} = 10^{-15}\ cm^2/s$, $D_{UPu}^{O} = 3*10^{-16}\ cm^2/s$, $D_{PuU}^{O} = 5*10^{-16}\ cm^2/s$, $D_{PuPu}^{O} = 10^{-16}\ cm^2/s$ whereas those that will reproduce the concentration profile of $U_{0.55}Pu_{0.45}O_2$ are: $D_{UU}^{O} = 10^{-14}\ cm^2/s$, $D_{UPu}^{O} = 10^{-15}\ cm^2/s$, $D_{PuU}^{O} = 8*10^{-15}\ cm^2/s$, $D_{PuPu}^{O} = 12 * 10^{-15}\ cm^2$.

in

2.3. Initial Conditions

Like every time-dependent problem, the first step is the definition of initial conditions, which define the composition of each single-crystal (each diffusion half-couple).

- **Case of UO_2/PuO_2**

The first half-couple is uranium dioxide. In the fluorine structure (case of UO_2), the expression of concentration is:

$$c = \frac{n}{V} = \frac{z}{N_a * a^3}$$

c is the concentration of U in the fluorine structure, z is the number of formula units in the conventional cell and its value is 4 for the UO_2 system, N_a is the Avogadro number. The lattice parameter a is 5.47Å at sintering temperature (around 1600 or 1700°C) [30]. The corresponding concentration of U is 0.04 mol/cm^3. By analogy, the lattice parameter of PuO_2 is 5.396Å and the concentration of Pu is 0.042 mol/cm^3. Those initial conditions are applied to solve the previous equations.

- **Case of $UO_2/U_{0.55}Pu_{0.45}O_2$**

The initial conditions of this couple are also required because they will be used at the step of validation of our model based on Dirichlet boundary conditions. The values of the initial concentrations of the first half-couple UO_2 at the left-hand side are

identical to those shown above: $c_U = 0.04 mol/cm^3$ and $c_{Pu} = 0$. Concerning the half-couple $U_{0.55}Pu_{0.45}O_2$ on the right-hand side, the concentrations of U and Pu are respectively: $c_U = \frac{1-y}{V_m}$ and $c_{Pu} = \frac{y}{V_m}$, where *y* is the Pu content, V_m the molar partial volume, $V_m = a^3(1+\alpha_T)^3 N_a$. The lattice parameter *a* is given by $a = 5.470 - 0.074y + (0.301 + 0.11y)x$ Å [32], with *x* the deviation from oxygen stoichiometry.

Taking into account a 45at%Pu content, the lattice parameter becomes 5.436Å. The thermal expansion coefficient α_T, for this non-stoichiometric component is: $\alpha_T = 1.1833 \times 10^{-5} - 5.013 \times 10^{-9}T + 3.756 \times 10^{-12}T^2 - 6.125 \times 10^{-17}T^3$ for 923≤T≤3120 K, leading to $c_U = 0.02273\ mol/cm^3$ $c_{Pu} = 0.0186\ mol/cm^3$.

2.4. Boundary conditions

Boundary conditions are required to close previous system of equations. The choice of the type of boundary conditions depends on the type of problem to be solved.

- **Dirichlet boundary conditions**

For the sintering of large single-crystals, because interdiffusion zone is smaller than the sample, Dirichlet boundary conditions will be first used. Note that the finite difference scheme that will be used later does not define the concentration values at the two external nodes, corresponding to k=1 and k=n. The Dirichlet boundary conditions considered here assume that the concentration in U and Pu does not change at the boundaries of spatial domain.

- **Neumann boundary conditions**

The Neumann boundary conditions consists in imposing the normal flux of the species at the boundary of the domain. Here, a flux equal to zero is considered, which means, in a 1D-situation, that no matter moves through the ends of the sample.

2.5. Numerical resolution of the problem: the finite difference discretization

This section describes the numerical method used for solving multicomponent diffusion partial differential equations. Diffpack library [29] is used in order to solve the resulting linear system of equations. The purpose is to analyze the evolution of concentration profiles of U and Pu chemical elements.

A finite difference scheme is applied to Equation 8, in order to approximate the unknown *c'* and then rebuild *c*. More precisely, the time domain [0, T] is discretized by a set of ordered points, $t_0=0, t_1, \ldots, t_n$, equally spaced. The time step is then defined by $\Delta t = t_l - t_{l-1}$ for any $l > 0$. Similarly, the space domain is discretized by a set of equidistributed points $x_1 = 0, x_2, \ldots, x_n$, with $x_{k+1} > x_k$ for any $k > 0$, spaced by $\Delta x = x_{k+1} - x_k$. With these notations, $c'(x_k, t_l)$ is approximated by $c'_{k,l}$. These coefficients are given by

$$\begin{cases} c'_{k,l+1}(U) = \lambda_U \times \frac{\Delta t}{\Delta x^2} c'_{k-1,l}(U) + (1 - 2\lambda_U \times \frac{\Delta t}{\Delta x^2}) c'_{k,l}(U) + \lambda_U \times \frac{\Delta t}{\Delta x^2} c'_{k+1,l}(U) \\ c'_{k,l+1}(Pu) = \lambda_{Pu} \times \frac{\Delta t}{\Delta x^2} c'_{k-1,l}(Pu) + (1 - 2\lambda_{Pu} \times \frac{\Delta t}{\Delta x^2}) c'_{k,l}(Pu) + \lambda_{Pu} \times \frac{\Delta t}{\Delta x^2} c'_{k+1,l}(Pu) \end{cases} \quad 2 \le k \le n-1 \qquad (8)$$

given by

$$\begin{cases} c_U = b_{UU} c'_U + b_{UPu} c'_{Pu} \\ c_{Pu} = b_{PuU} c'_U + b_{PuPu} c'_{Pu} \end{cases} \qquad (9)$$

by

One of the most important steps of the resolution of time-dependent problem is the choice of the time step. In the explicit schemes, the Courant-Friedrichs-Lewy (CFL) condition requires that the number of Courant be less than *0.5*. This number is defined for a one-dimensional system by: $C = \lambda_U \times \frac{\Delta t}{\Delta x^2}$ or $C = \lambda_{Pu} \times \frac{\Delta t}{\Delta x^2}$. Thus, the value assigned to C is *0.3*. Knowing the value of λ_U and λ_{Pu}, the value of time step is deduced, which is the minimum between $\frac{C \times \Delta x^2}{\lambda_U}$ and $\frac{C \times \Delta x^2}{\lambda_{Pu}}$. The value of space step is $\Delta x = L/(n-1)$, with *L* the length throughout the two half-couples and *n* is the total number of discretization points. This finite difference scheme is associated with the Dirichlet boundary conditions, which can be written in terms of the finite difference scheme as follows:

$c'_{1,l+1}(U) = c'_{1,l}(U)$ $\qquad$ $c'_{1,l+1}(Pu) = c'_{1,l}(Pu)$

differe

$c_{1,l+1}$(U)= $b_{UU}\times c'_{1,l+1}$(U)+ $b_{UPu}\times c'_{1,l+1}$(Pu)

$c_{1,l+1}$(Pu) =$b_{PuU}\times c'_{1,l+1}$(U)+$b_{PuPu}\times c'_{1,l+1}$(Pu)

$c'_{n,l+1}$(U)= $c'_{n,l}$(U)

$c'_{n,l+1}$(Pu)= $c'_{1,l}$(Pu)

$c_{n,l+1}$(U)= $b_{UU}\times c'_{n,l+1}$(U)+ $b_{UPu}\times c'_{n,l+1}$(Pu)

$c_{1,l+1}$(Pu) =$b_{PuU}\times c'_{n,l+1}$(U)+$b_{PuPu}\times c'_{n,l+1}$(Pu)

Therefore, the system is solved numerically and the unknown concentrations are then deduced.

Concerning the numerical implementation based on Neumann boundary conditions, the mathematical equations can be written:

$\nabla c = 0$ at *k=1* and *k=n* . This leads to $\nabla c' = 0$ at *k=1* and *k=n*. Assuming that at the end point at *k = 1*, the incoming flux is equal to the outgoing flux: $c'_{1,l+1}(U) = \lambda_U \times \frac{\Delta t}{\Delta x^2}(c'_{0,l}(U) - 2\times c'_{1,l}(U) + c'_{2,l}(U)) + \lambda_U \times \frac{\Delta t}{\Delta x^2} c'_{1,l}(U)$. The condition of flux null is applied between the point k=1 and a point out of the domain k=0. Assuming that the difference between the flux at k=1 and at the other outer points on the left is zero at all times. This means that $c'_{1,l}(U) - c'_{0,l}(U) = 0$. The concentration $c'_{0,l}$ is the concentration at a point out of the domain. By replacing $c'_{0,l}(U) = c'_{1,l}(U)$ in the previous relation, the deduction appears $c'_{1,l+1}$(U) = (1 - $\lambda_U \times \frac{\Delta t}{\Delta x^2}$) $c'_{1,l}$(U) + $\lambda_U \times \frac{\Delta t}{\Delta x^2} c'_{2,l}$(U). The process is the same for point k = n.

Thus, at the first point corresponding to k=1, $c'_{1,l+1}$(U) = (1 - $\lambda_U \times \frac{\Delta t}{\Delta x^2}$) $c'_{1,l}$(U) + $\lambda_U \times \frac{\Delta t}{\Delta x^2} c'_{2,l}$(U)

At the last one corresponding to k=n, $c'_{n,l+1}$(U) = $\lambda_U \times \frac{\Delta t}{\Delta x^2} c'_{n-1,l}$(U) + (1 − $\lambda_U \times \frac{\Delta t}{\Delta x^2}$)$c'_{n,l}$(U)

By analogy, $c'_{1,l+1}$(Pu) = (1 - $\lambda_{Pu} \times \frac{\Delta t}{\Delta x^2}$) $c'_{1,l}$(Pu) + $\lambda_{Pu} \times \frac{\Delta t}{\Delta x^2} c'_{2,l}$(Pu)

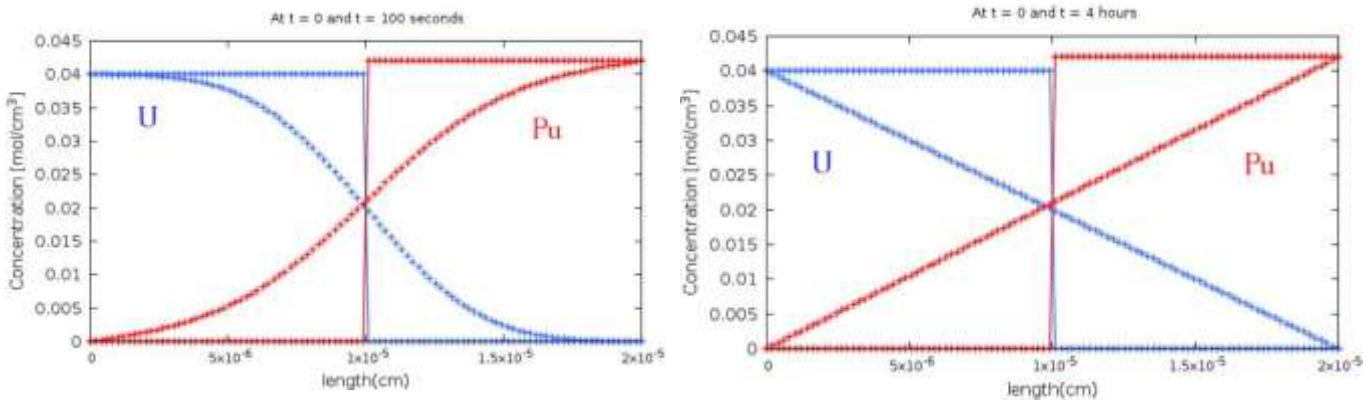
$c'_{n,l+1}$(Pu) = $\lambda_{Pu} \times \frac{\Delta t}{\Delta x^2} c'_{n-1,l}$(Pu) + (1 − $\lambda_{Pu} \times \frac{\Delta t}{\Delta x^2}$)$c'_{n,l}$(Pu)

These resulting equations associated with the finite difference scheme lead to a numerical system that is solved using the functionalities of the Diffpack library for the finite difference method.

3. Results and discussion

3.1. simulation of two single-crystals of UO_2 and PuO_2

So far, the physical model and the numerical method necessary to solve the interdiffusion phenomenon between two single-crystals in contact were presented. The purpose is to find the unknown concentrations of U and Pu as a function of time. As mentioned at the beginning of this paper, we aim at analyzing the change in concentration of each chemical element during interdiffusion in a system constituted by two half-couples of single-crystals. One made of UO_2 and the other PuO_2. Based on the fact that the size of these crystallites as shown by scanning electron microscope or deduced from X-Rays peak width in diffraction patterns, lies between 100 and 300nm, we have simulated the interdiffusion using the size of 100nm. Thus, the entire length of the two half-couples is 200nm. The initial interface separating the two half-couples is located in the center of the domain. Figure 1 shows the evolution of the concentration of each chemical element when two single-crystals (assumed as being crystallites) of UO_2 and PuO_2 are brought into contact. Dirichlet boundary conditions were first used.



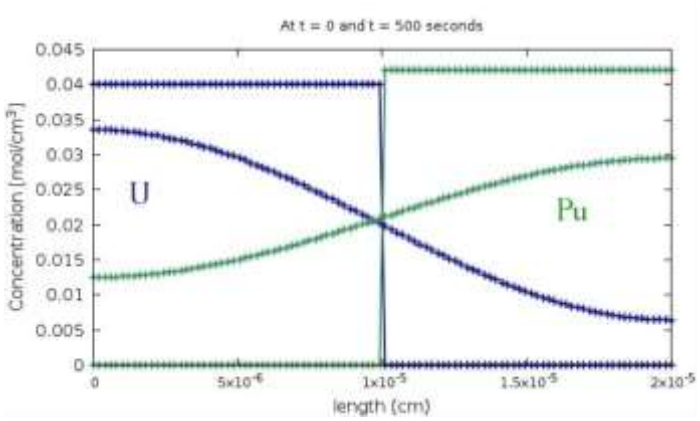
a) *During the first 100 seconds* b) *During the first four hours*

Figure 1 : Concentration profiles of U and Pu as a function of distance between the two half-couples of interdiffusion using Dirichlet boundary conditions

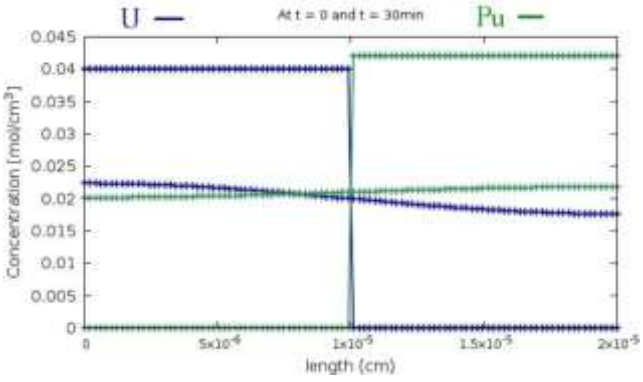
This Figure shows the interdiffusion phenomenon. Initially, UO_2 occupies only the left half-couple, and PuO_2 occupies the right hand half (Figure 1.a). These sharp concentrations are quickly smoothed out, due to the diffusion regularization effect, or mathematically, the Laplacian term in Fick's law (Figure 1.a). The mole number of each species, *i.e.* the area under each curve, is conserved over time. Since the concentration of Pu and U is imposed at both domain boundaries, the steady state is reached with the straight profiles shown in Figure 1.b: the time derivative is equal to zero, and consequently the spatial second-order derivative of the concentration is also equal to zero.

This computation allows to highlight the manifestations of diffusion phenomena at any points of the single-crystals, except at the ends points. The other observation is that the complete diffusion takes less than 4 hours: the interdiffusion totally occurs during the sintering. However, the values of concentration at the ends, which remain fixed during the interdiffusion, do not represent the physical reality of interdiffusion within crystallites. An alternative would be to use another type of boundary condition based on the zero flux of each element at the ends of the domain: the Neumann boundary conditions described above (paragraph 2.4).

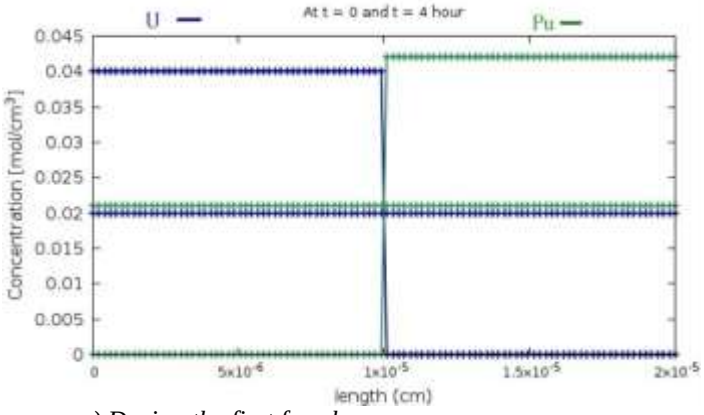
The numerical implementation of Neumann boundary conditions as described above allows us to plot the concentration profiles of U and Pu shown in Figure 2 :



a) *During the first 500 seconds*



b) During the first 30 minutes



c) During the first four hours

Figure 2 : Concentration profiles of U and Pu as a function of distance between the two half-couples of interdiffusion using Neumann boundary conditions

The same remarks as previously mentionned apply: the diffusion effect appears clearly, while the mole number of each species is well preserved. Since the space derivative of both concentrations are set to zero at the boundaries of the domain, the steady state is a state of constant concentration. The Neumann boundary conditions give a good description of the physical reality of interdiffusion at the crystallite scale during sintering when the interdiffusion zone is significant in comparison to the total interdiffusion couple length.

3.2. Validation of the model based on Dirichlet boundary conditions

The Dirichlet boundary conditions used to simulate the interdiffusion between two single-crystals do not represent the reality of phenomena because the size of single-crystals and the interdiffusion zone are of the same order of magnitude. In contrast, we can use this type of boundary conditions when the interdiffusion zone is smaller than the entire length constituted by the two half-couples, for example the case of the single-crystals with bigger size. Therefore, in order to validate our model, we will try to reproduce the results acquired during an experiment based on two interdiffusion half-couples, one consisting of a pure UO_2 half pellet, the other one consisting of a half-pellet of the mixed oxide $U_{0.55}Pu_{0.45}O_2$. In this aim, the initial conditions as described at Section 2.3 are used. The required interdiffusion coefficients were presented with the physical model (see Section 2.2).

So far, the only work in the literature dealing with the concentration profiles of UO_2 and $U_{0.55}Pu_{0.45}O_2$ is that of Noyau [28]. He plotted the evolution of concentration as a function of distance along the interdiffusion couple. To cope with the very limited interdiffusion zone which extends from 2 up to 5 µm, the author selected an acquisition line for concentration measurements by means of a Castaing EPMA (Electron Probe Micro Analyzer) making a very small α angle with the bonding interface of the two half-pellets. He managed in this way to obtain a large number of points with varying concentrations within the interdiffusion zone. The total distance between extreme acquisition points measured perpendicular to the bonding interface remains very small compared to the total length of the half-couples. Therefore, Dirichlet boundary conditions can be applied to these two half-couples to simulate U-Pu interdiffusion.

For a temperature of 1700°C and 50 hours of interdiffusion, the inclination angle is α=2,048 × 10^{-2}rad. In the second case where the duration of interdiffusion is 143 hours, the inclination angle is 3,175 × 10^{-2} rad. Figure 3 shows the two half-couples as well as the position of the acquisition line in relation to the bonding interface separating the two half-couples as described by Noyau [28].

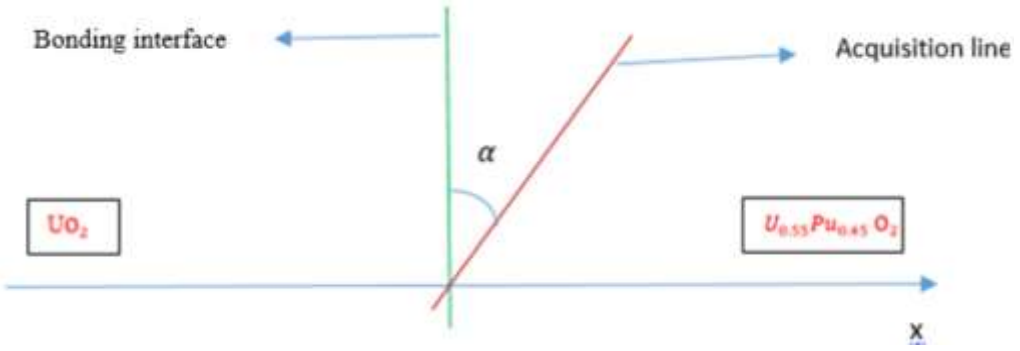


Figure 3 : Position of the acquisition line in relation to the bonding interface separating the two half-couples $UO_2/U_{0.55}Pu_{0.45}O_2$

The interdiffusion between UO_2 and $U_{0.55}Pu_{0.45}O_2$ has been simulated for two durations of interdiffusion: 50 and 143 hours. The interdiffusion profiles are then compared to the experimental results of Noyau as shown on Figure 4.

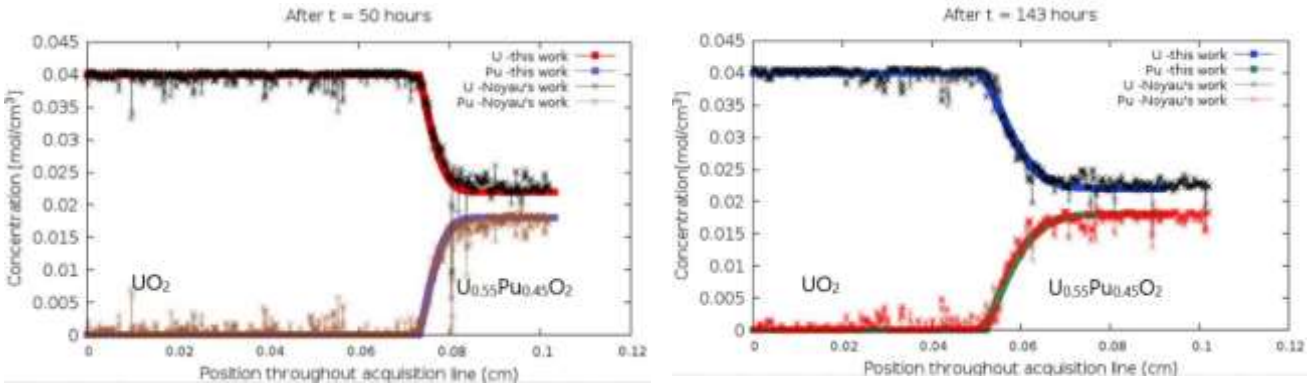


Figure 4 : Concentration profiles of elements U and Pu at 1700°C after 50 hours and after 143 hours

In each figure, a good agreement can be observed between experiments and simulation, although some peaks can be observed on experimental results, probably due to grains boundary diffusion in the polycrystalline materials used. Such an agreement

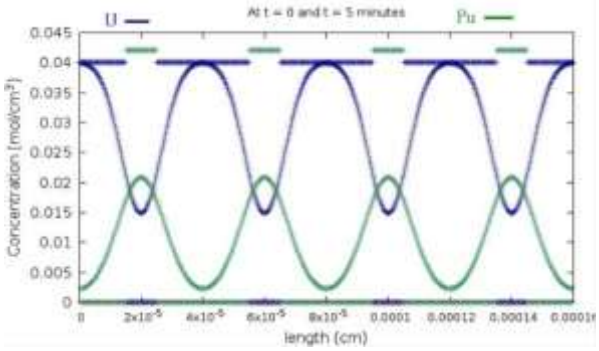
with experimental results validates the numerical model based on Dirichlet boundary conditions used for pellets or very large single-crystals in which interdiffusion zone is smaller than the total sample size.

3.3. Numerical study of homogenization within two microstructures

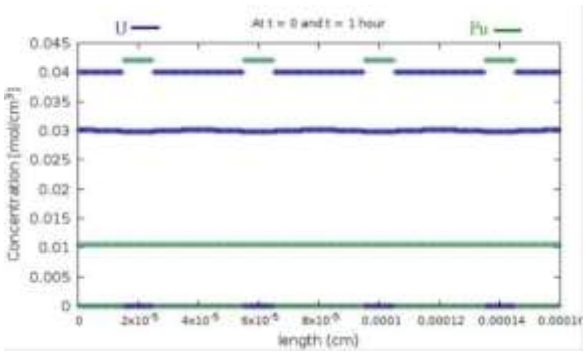
The second part of the results obtained in this paper is the evolution and the achievement of the homogenization in two different microstructures. The realistic simulation of sintering can be extended to more than two single-crystals or grains; it is a question of analyzing the homogenization phenomenon upon a set of grains consisting initially of UO_2 and PuO_2. The aim of this part is firstly, to better qualify this phenomenon with a given criterion of homogeneity and secondly, to compare the time of homogenization in different types of microstructures. Because of small size of single-crystals and in order to solve correctly the numerical problem, the Neumann boundary conditions will be used. Neumann conditions result in the nullity of flux in the center of each ending single-crystals, which are symmetry planes. Two types of microstructures will be studied: a unimodal distribution microstructure and a non-unimodal distribution microstructure of UO_2 and PuO_2.

- **A unimodal distribution of UO_2 and unimodal distribution of PuO_2**

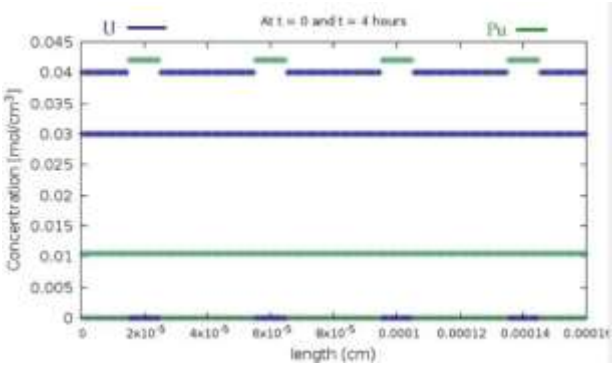
During the step of grinding (step prior to sintering), the mechanical properties playing a role for UO_2 crystallites are different from those of PuO_2. As a consequence, UO_2 crystallites are generally larger in size than those of PuO_2. The first microstructure under consideration that appears is a set of single-crystals with various sizes: 300nm for UO_2 single-crystals and 100nm for PuO_2. Each type of assembly consists of four single-crystals. The size of the single-crystals at the ends is half of that of the corresponding crystal in order to represent a periodic infinite microstructure. For this microstructure, the concentration profiles are shown in
Figure 5:



a) During the first five minutes



b)During the first hour



c) During the first four hours

Figure 5 : concentration profiles at different times

After 5 minutes, the concentration, which was initially discontinuous at the grain boundary and constant in each grain, becomes smooth and remains periodic. This behavior highlights the effect of the diffusion phenomenon. A distribution of the concentration of each element upon the entire sample length is observed over time. After 1 hour, the profiles present a repartition of each chemical element, which can indicate that homogenization takes place. After 4 hours, a "steady state" seems to be reached. However, the time of the exact achievment of a satisfactory homogeneous mixing cannot be stated with certainty. To reach this goal, a homogeneity criterion will be used.

The homogeneity criterion depends on the scale of observation. In the 1D-representation of this work, this scale, h_k, can simply be specified with respect to the space step Δx: $h_k = 2^k \times \Delta x$, with $0 \leq k \leq \frac{ln(n)}{ln(2)} - 1$, n is the number of points of the spatial discretization. In the following, the scale of observation will be the scale given by the spatial discretization, *i.e.* $h_0 = \Delta x$. At this scale, the standard deviation σ, *i.e.* the deviation from the average of concentration, is proposed as criterion. It has the same unity as the concentration, and its meaning is easy to interpret. For a Δx scale, the standard deviation is written as:

$$\sigma(\Delta x) = \sqrt{\frac{1}{n}\sum_{i=1}^{n}(c_U(i) - \bar{c}_U)^2} \quad (10)$$

The plot of σ on a logarithm scale versus time on a linear scale leads to the graphs presented over the first four hours in Figure 6:

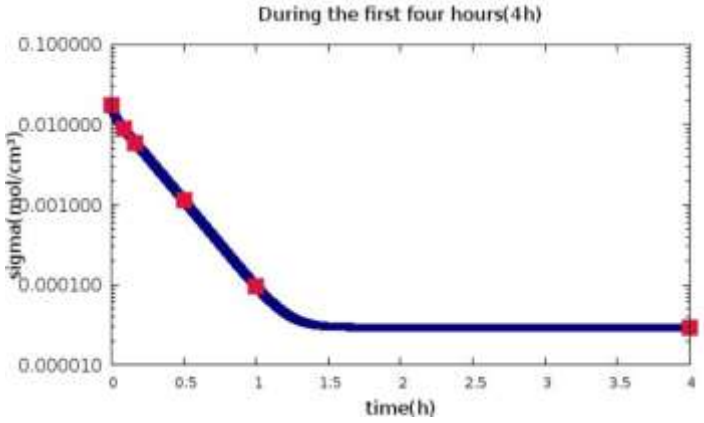
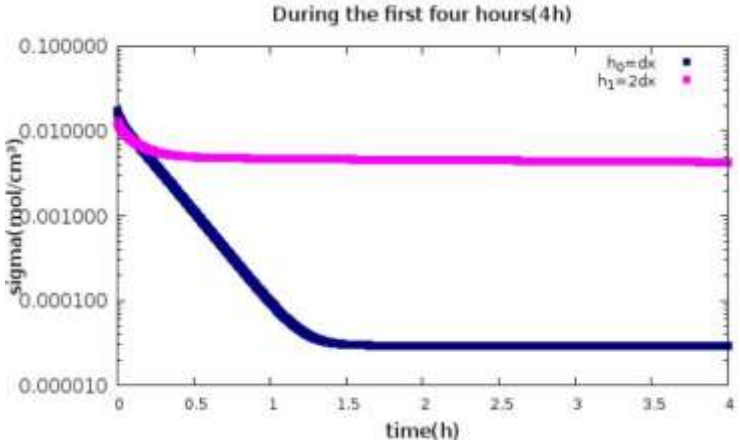


Figure 6 : Evolution of standard deviation σ on a Δx observation scale as a function of time

The standard deviation decreases. This decrease is continuous and sigma becomes constant from 1.5 hour on, which corresponds to the smallest value of σ ($2.93*10^{-5}$mol/cm^3). The plateau at this value of sigma starting at 1.5 hour can lead to conclude to a satisfactory homogeneity of the system after 4 hours of interdiffusion. The red squares on the curve stand for the values of sigma at each time corresponding to the different curve of concentration represented in ***Erreur ! Source du renvoi introuvable.****. The plateau tends towards a horizontal asymptote close to 0 and not 0 due to the local truncation error of the numerical scheme [33]. This kind of error is frequently encountered in the numerical*



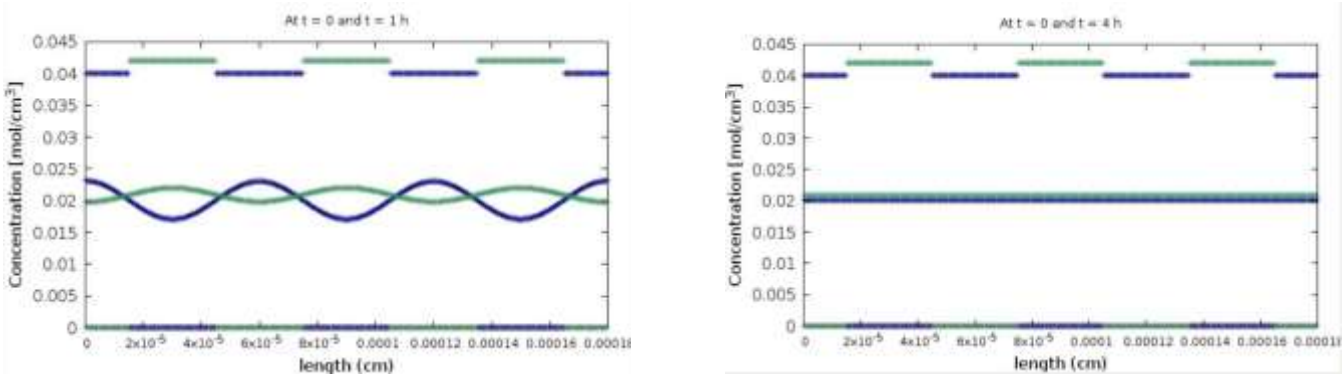
resolutions. If the spatial discretization step increases (2Δx for example), the value of σ will increase. The curve of σ quickly becomes flat and the plateau corresponds to a σ value ($4.31*10^{-3}mol/cm^3$) greater than the scaled value Δx. The representations of sigma versus time for a discretization of 2Δx (

Figure 7) can be used to assert that there is no consistency error. It emerges from these analyses that for this specific size and unimodal distribution of UO_2 as well as unimodal distribution of PuO_2, a significant homogenization occurs and ends within the duration of sintering.

Figure 7 : Evolution of standard deviation σ on a 2Δx discretization scale as a function of time

- **A unimodal distribution of UO_2 and PuO_2**

Before dealing with the second microstructure, we analyze the time to achieve a satisfactory homogenization time in the case in which the two single-crystals have the same size. The size of PuO_2 crystallite becomes 300nm like UO_2 size. As previously, UO_2 is presented in blue and PuO_2 in green. The results are plotted in Figure 8:



a) *During the* first hour

b) During the first four hours

Figure 8: Concentration profiles at different times

As previously, we note the same change except that they occur later on. Moreover, the repartition of concentration of each chemical element along the entire length takes place at the same value of concentration, which is a consequence of the initial choice of single-crystals relative sizes. The representations of standard deviation on a logarithm scale versus time on a linear scale during the first 4 hours is shown in Figure 9:

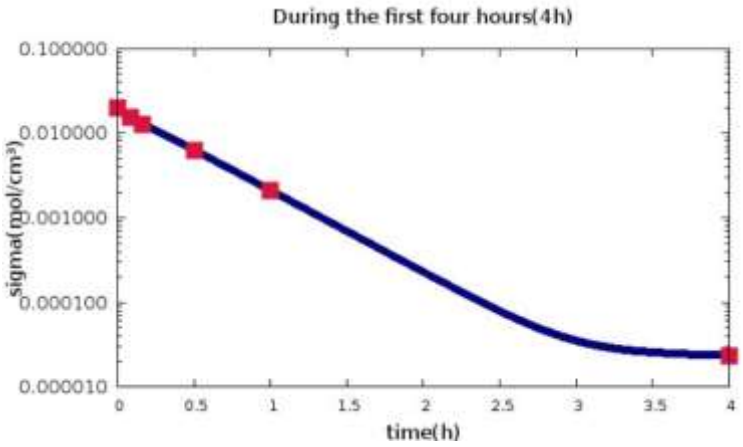


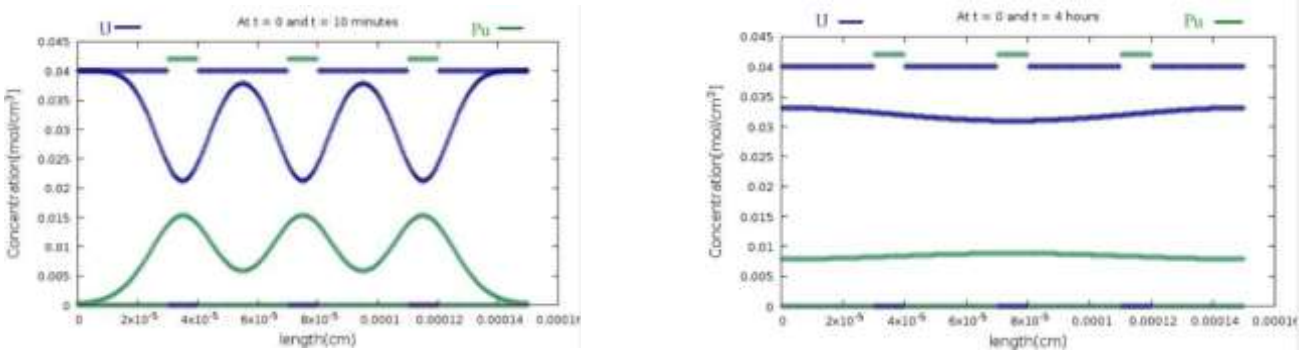
Figure 9 : Evolution of standard deviation σ on a Δx observation scale as a function of time

Homogeneity is achieved later than in the previous case. It comes from the fact that the mean crystallite size has increased whereas the diffusion coefficient remains the same. The value of sigma at the plateau is $2.35*10^{-5}$mol/cm^3, i.e. smaller than its value for a unimodal distribution of UO_2 and unimodal distribution of PuO_2. One of the interesting remarks is that this significant homogenization occurs during the duration of the sintering process. Therefore, the increase of the size of a type of single-crystal (PuO_2 in this case) delays the time to reach a significant homogenization.

- **A non-unimodal distribution of UO_2 and PuO_2**

The second microstructure consists of single-crystals with various sizes. The study will be divided into two parts: one consist of non-unimodal distribution with 25%Pu content and the other with 45% Pu content. Here, the Pu content stands for the proportion of PuO_2 within the entire length. The aim is to compare the time to reach a significant homogenization within these two microstructures.

That of 25% consists of six single-crystals of UO_2 and three of PuO_2. Two of UO_2 measure 300nm in size and while the two others measure 600nm in size. The two single-crystals of UO_2 with 600nm are represented at the ends. On the other hand, all PuO_2 crystallites measure 100nm in size. The numerical method (finite difference scheme), the initial conditions (c_U = *0.04mol/l and* c_{Pu} = *0.042mol/l*) and the boundary conditions (Neumann boundary conditions) are identical as in the previous section. The plots are presented on Figure 10:

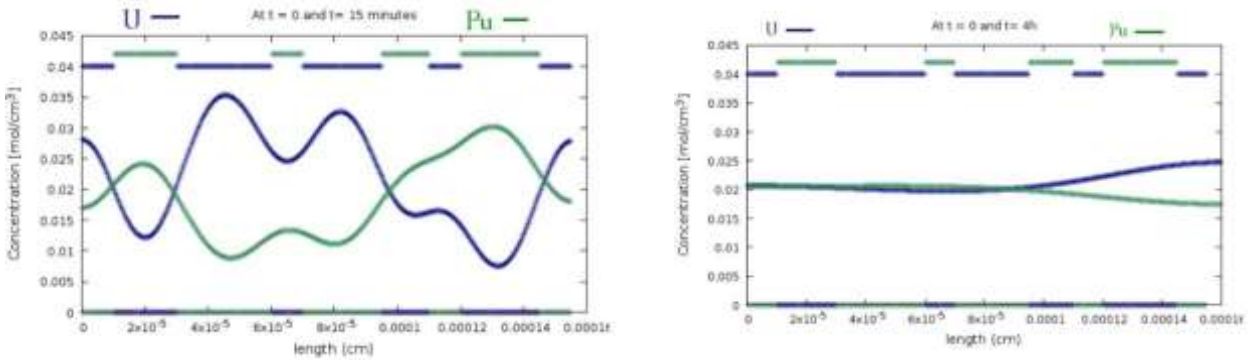


a) *During the first ten minutes* *b) During the first four hours*

Figure 10 : Concentration profiles at different time

In this case, achieving the homogenization seems to take longer than in previous cases due to the larger mean size. After four hours, the concentration profile is not yet constant as it was in the case of unimodal distribution. This representation can demonstrate a lot in the non-achievement of homogenization, but is not sufficient to analyze it quantitatively.

On the other hand, the plot of concentration profile for the other of 45% Pu content is shown in Figure 11. Its consists of four single-crystals of UO_2 (300nm, 250nm, 200nm and 100nm) and four of Puo_2 (250nm, 200nm, 150nm and 100nm).



a) *During the first fifteen minutes* *b) During the first four hours*

Figure 11 : Concentration profiles at different time

Figure 10 and Figure 11 confirm the idea of the presence of heterogeneity after the first four hours in those two non-unimodal distribution. Figure 12 shows the standard deviation of these two non-unimodal microstructures in order to compare them quantitatively.

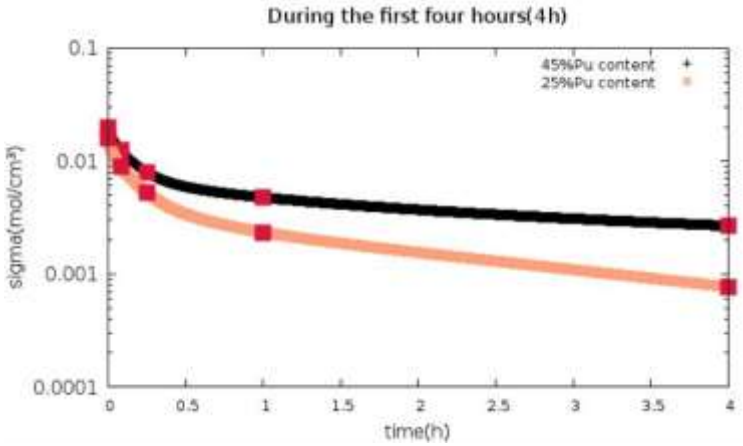


Figure 12 : Standard deviation of non-unimodal distribution microstructure with 45%Pu and 25%Pu content

The behavior of the concentration standard deviation curve of the two microstructures are identical. However, the microstructure with 25%Pu content decreases more quickly compared to that with a 45% Pu content. The value of standard deviation of microstructure with 25%Pu content is $7.68*10^{-4}$mol/cm^3 whereas the other one is $2{,}66 * 10^{-3}$mol/cm^3. Note that, at these two values, a significant homogenization is not yet achieved. Using the relation $x = \sqrt{Dt}$ which relates the characteristic distance and interdiffusion time, the time necessary to achieve interdiffusion can be calculated. In this study, $x = \sqrt{\lambda t}$, where λ is the smallest value between λ_U and λ_{Pu}. Thus, for the size of 300nm, the time is: $t = (300 \times 10^{-7})^2 / 5.68338 \times 10^{-14} \approx 4.4$ hours. Microstructures showing several single-crystals with large size increases the achieving homogenization time. From these analyses, the influence of the grain size can be one of the cause of this later achievement of a significant homogeneity.

4. Conclusion

The paper has dealt with the interdiffusion phenomena observed during mixed oxides sintering. The multicomponent diffusion principle and the numerical method used to simulate U and Pu diffusion in $(U,Pu)O_2$ were presented. We first noted a good agreement between our work using Dirichlet boundary conditions and the experimental work by Noyau with half-pellets used as interdiffusion couples, which allows us to validate the simulation of interdiffusion for large size samples. From a mathematical point of view, we have shown that taking into account the zero-flux Neumann boundary conditions is a good representation of the reality of interdiffusion (mass conservation) at the scale of crystallites. The numerical resolution was carried out using a finite difference scheme. Then, the second part of this study of homogenization within different types of microstructures allowed to highlight and use a homogeneity criterion which is the standard deviation of one of the diffusing

species. The standard deviation of concentration was useful to quantify the achievement of the homogeneity within a microstructure. Finally, in this entire framework, only volume diffusion coefficients were used, since the simulations were carried out in one dimension. In a future 2D and 3D-work, we will also take into account grain-boundary diffusion, which is not negligible at lower temperatures and contributes strongly to diffusion phenomena. This part will constitute the next goals in the development of our reactive sintering model. This scheme of simulation of interdiffusion will be implemented together with the mechanical model into the sintering model (SALAMMBO) developed in our laboratory in order to able to simulate the reactive sintering of MOX fuel.

References

[1] E. B. Slamovich et F. F. Lange, « Densification Behavior of Single-Crystal and Polycrystalline Spherical Particles of Zirconia », *J. Am. Ceram. Soc.*, vol. 73, nº 11, p. 3368-3375, nov. 1990, doi: 10.1111/j.1151-2916.1990.tb06463.x.

[2] P. Descamps, S. Sakaguchi, M. Poorteman, et F. Cambier, « High-Temperature Characterization of Reaction-Sintered Mullite-Zirconia Composites », *J. Am. Ceram. Soc.*, vol. 74, nº 10, p. 2476-2481, oct. 1991, doi: 10.1111/j.1151-2916.1991.tb06788.x.

[3] S. Prochazaka, J. S. Wallace, et N. Claussen, « Microstructure of Sintered Mullite-Zirconia Composites », *J. Am. Ceram. Soc.*, vol. 66, nº 8, p. C-125-C-127, août 1983, doi: 10.1111/j.1151-2916.1983.tb10104.x.

[4] A. Raghdi, M. Heraiz, F. Sahnoune, et N. Saheb, « Mullite-zirconia composites prepared from halloysite reaction sintered with boehmite and zirconia », *Appl. Clay Sci.*, vol. 146, p. 70-80, sept. 2017, doi: 10.1016/j.clay.2017.05.037.

[5] C. Duran et Y. Kemal Tür, « Templated grain growth of textured mullite/zirconia composites », *Mater. Lett.*, vol. 59, nº 2-3, p. 245-249, févr. 2005, doi: 10.1016/j.matlet.2004.07.058.

[6] J. Rojek, S. Nosewicz, M. Maździarz, P. Kowalczyk, K. Wawrzyk, et D. Lumelskyj, « Modeling of a Sintering Process at Various Scales », *Procedia Eng.*, vol. 177, p. 263-270, 2017, doi: 10.1016/j.proeng.2017.02.210.

[7] D. Pino-Muñoz, J. Bruchon, S. Drapier, et F. Valdivieso, « Sintering at Particle Scale: An Eulerian Computing Framework to Deal with Strong Topological and Material Discontinuities », *Arch. Comput. Methods Eng.*, vol. 21, nº 2, p. 141-187, juin 2014, doi: 10.1007/s11831-014-9101-4.

[8] F. Wakai, G. Okuma, et N. Nishiyama, « Sintering mechanics of ceramics: a short review », *Mater. Today Proc.*, vol. 16, p. 4-13, 2019, doi: 10.1016/j.matpr.2019.05.304.

[9] W. Zhang et I. Gladwell, « Sintering of two particles by surface and grain boundary diffusion – a three-dimensional model and a numerical study », *Comput. Mater. Sci.*, vol. 12, nº 2, p. 84-104, sept. 1998, doi: 10.1016/S0927-0256(98)00035-4.

[10] W. Zhang et J. H. Schneibel, « The sintering of two particles by surface and grain boundary diffusion—a two-dimensional numerical study », *Acta Metall. Mater.*, vol. 43, nº 12, p. 4377-4386, déc. 1995, doi: 10.1016/0956-7151(95)00115-C.

[11] M. Ajdour, « Développement d'un code de calcul pour la simulation du frittage en phase solide. PhD. thesis - science et génie des matériaux », Ecole Nationale Supérieure des Mines de Saint-Etienne, 2006.

[12] J. Léchelle, S. Martin, R. Boyer, et K. Saikouk, « A sub-granular scale model for solid state free sintering: results on the evolution of two grains », *Journal of Chemical Technology and Metallurgy, 49, 3, 2014, 263-274.*

[13] J. Léchelle, R. Boyer, et M. Trotabas, « A mechanistic approach of the sintering of nuclear fuel ceramics », *Mater. Chem. Phys.*, vol. 67, nº 1-3, p. 120-132, janv. 2001, doi: 10.1016/S0254-0584(00)00429-6.

[14] L. S. Darken, « Application of the Gibbs-Duhem Equation to Ternary and Multicomponent Systems », *J. Am. Chem. Soc.*, vol. 72, nº 7, p. 2909-2914, juill. 1950, doi: 10.1021/ja01163a030.

[15] E. L. Cussler, *Multicomponent diffusion - Chemical Engineering Monographs 3*, Elsevier Scientific Publishing Company., vol. 3. Amsterdam - Oxford - New York, 1976.

[16] J. Philibert, *Diffusion et transport de matière dans les solides*, Les éditions de Physique. .

[17] M. Kajihara. Kikuchi, « Analysis of dissolution of alpha phase in gamma/alpha/gamma Diffusion couples of the Fe-Cr-Ni system using analytical solutions for semi-infinite diffusion couples »,*Acta Metall Mater, Vol 43*

[18] J. M. Vitek, S. A. Vitek, et S. A. David, « Numerical modeling of diffusion-controlled phase transformations in ternary systems and application to the ferrite/austenite transformation in the Fe-Cr-Ni system », *Metall. Mater. Trans. A*, vol. 26, nº 8, p. 2007-2025, août 1995, doi: 10.1007/BF02670673.

[19] D. Glasser-Leme et H. Matzke, « Dependence upon oxygen potential of the interdiffusion in single crystallite U02-(U, Pu)O2 », Solid State Ionics 12, (1984) 217-225

[20] P. Jean Baptiste et G. Gallet, « Interdiffusion des cations dans les oxydes mixtes (U, Ce)O2- x et (U, Pu)O2-x; Influence de la teneur en uranium, de la temperature et de l'écart à la stoechiométrie. », *J. Nucl. Mater.*, 1985.

[21] D. Glasser-Leme et H. Matzke, « Interdiffusion and chemical diffusion in the uo2 - (u,pu)o2 system », *J. Nucl. Mater.*, vol. 106, p. 211-220.

[22] R. Verma, « Study of homogenisation and cation interdiffusion in mixed UO2-PuO2 compacts by x-ray diffraction », *Journal of Nuclear Materials*, p. 9.

[23] S. Mendez, S. Pillon, D. Warin, et R. Lorenzelli, « Diffusion Cationique et Croissance Cristalline à l'Interface UO2-PuO2 », *J. Phys. IV*, vol. 05, nº C3, p. C3-297-C3-303, avr. 1995, doi: 10.1051/jp4:1995330.
[24] S. Berzati *et al.*, « Controlling the oxygen potential to improve the densification and the solid solution formation of uranium–plutonium mixed oxides », *J. Nucl. Mater.*, vol. 447, nº 1-3, p. 115-124, avr. 2014, doi: 10.1016/j.jnucmat.2013.12.014.
[25] T. Kanit, S. Forest, I. Galliet, V. Mounoury, et D. Jeulin, « Determination of the size of the representative volume element for random composites: statistical and numerical approach », *Int. J. Solids Struct.*, p. 33, 2003.
[26] A. E. Moumen, « Numerical evaluation of the representative volume element for random composites », *Eur. J. Mech.*, p. 8, 2021.
[27] Bernache-Assollant, « Chimie-Physique du frittage », Hermes Eds., 1993, p. 348.
[28] S. Noyau, « Etude des phénomènes d'autodiffusion et d'interdiffusion du plutonium dans les céramiques de type U1-yPuyO2±x », Thèse de l'Université de Limoges, 2012.
[29] H. P. Langtanten, *Computational Partial Differential Equations*, vol. tome 2. .
[30] J. Andersson et J. Ågren, « Models for numerical treatment of multicomponent diffusion in simple phases », *J. Appl. Phys.*, vol. 72, nº 4, p. 1350-1355, août 1992, doi: 10.1063/1.351745.
[31] H. Matzke, « Atomic Transport Properties in U 0 2and Mixed Oxides (U,Pu)O2 », *J Chem S*, p. 23.
[32] « Thermodynamic and transport properties of Uranium dioxide and related phases », International atomic energy agency, Vienna, 1965.
[33] H. P. Langtangen et S. Linge, *Finite Difference Computing with PDEs: A Modern Software Approach*, vol. 16. Cham: Springer International Publishing, 2017.